Check for updates

Biofunctional few-layer metal dichalcogenides and related heterostructures produced by direct aqueous exfoliation using phospholipids†

Aled T. Williams,[a] Roberto Donno, [ID][b] Nicola Tirelli[b] and Robert A. W. Dryfe [ID]*[ac]

We report a novel, inexpensive and green method for preparing aqueous dispersions of various biofunctional transition-metal dichalcogenides (MoS_2, WS_2, TiS_2 and $MoSe_2$) and their related heterostructures directly *via* ultrasonic exfoliation mediated by the presence of phospholipids. The dispersions predominantly consist of few-layer flakes coated with 1,2-dioleoyl-*sn-glycero*-3-phosphocholine (DOPC), as confirmed by Raman, photoluminescence and X-ray photoelectron spectroscopies. The phospholipid coating renders the flakes biofunctional, which coupled with the unique properties of transition-metal dichalcogenides and their heterostructures, suggests this method will have great potential in biological applications.

Transition-metal dichalcogenides (TMDCs) and other species of layered inorganic compounds are currently attracting much interest as the next generation of two-dimensional (2D) materials beyond graphene.[1] These materials, notably MoS_2, WS_2 and hexagonal boron nitride (hBN), have already found applications in fields such as optoelectronics and energy storage due to their unique physical properties.[2–6] Structurally, TMDCs are 2D layers of transition metal atoms, M, each covalently bound to two chalcogen atoms, X, and held together by van der Waals forces. The combination of metal and chalcogen influences the electronic properties of the material, for example TiS_2 is a semimetal whilst MoS_2 is a semiconductor in its naturally occurring, 2H, phase.[7] In addition to MX_2 compounds, similar structures are also embodied by hBN, Bi_2Te_3, transition-metal oxides, silicene, germanene and phosphorene (exfoliated black phosphorus) providing a range of new 2D materials for exploitation based on their individual attributes.[1,8] There is also growing interest in hetero-structures formed from these materials, *i.e.* stacked combinations of different 2D species, offering further diversity in the properties that can be harvested from these layered materials.[2,9–11]

Solution processing of 2D materials is essential for industrial applications[12] where the time-intensive and costly approaches of micromechanical cleavage and chemical vapour deposition

hinder the commercial viability of some technologies. Several liquid-phase exfoliation methods have been reported over recent years, the majority of which have been based on earlier methods applied to the exfoliation of graphite.[13,14] Notably, direct sonication of bulk powders in high boiling-point (HBP) solvents such as *N*-methyl-2-pyrrolidone (NMP) has been shown to produce monolayer to few-layer (layer number, $n \leq 3$) dispersions of TMDCs and other layered inorganic materials with reasonable stabilities and concentrations (up to 40 mg mL^{-1}).[15,16] However, direct sonication using HBP solvents raises obvious economic, environmental and safety concerns and furthermore, HBP solvent residues in thin films fabricated from such dispersions can be difficult to remove, which can be detrimental to subsequent applications in electronics.[17] Alternative preparation techniques, such as chemical and electrochemical Li-intercalation[18–20] and various surface functionalization strategies using organic molecules,[19,21] often involve multiple steps and undesirable reaction conditions.

Aqueous exfoliation methods can address many of these issues. However, successful liquid-phase exfoliation requires that the enthalpy of mixing per unit volume associated with the dispersal of the 2D flakes is close to zero, and it has been shown that for TMDCs[22] optimal solvents are characterized by surface tensions in the region of 40 mJ m^{-2}, with water falling outside this range at 72.75 mJ m^{-2} (at 20 °C).[23] However, aqueous dispersions of hydrophobic flakes can be stabilized electrostatically or sterically, and a number of recent reports detail the use of surfactants or polymers in facilitating the aqueous exfoliation of layered inorganic materials *via* the application of ultrasonic energy.[24–28] Herein, we report on a new exfoliation method, where phospholipids are used as electrostatic stabilizing agents in preparing aqueous dispersions of TMDCs

[a]School of Chemistry, University of Manchester, Oxford Road, Manchester, M13 9PL, UK. E-mail: robert.dryfe@manchester.ac.uk

[b]Laboratory of Polymers and Biomaterials, Fondazione Istituto Italiano di Tecnologia, Via Morego, 30, Genoa, Italy

[c]National Graphene Institute, University of Manchester, Oxford Road, Manchester, M13 9PL, UK

directly *via* sonication of the bulk materials. Phospholipids have the additional advantage of imparting bio-compatibility to the 2D materials. We also demonstrate that the mixing and subsequent sonication of these dispersions result in the formation of hetero-structured materials, whose optoelectronic characteristics can be modified by the respective ratios of the parent materials.

Briefly, our method involves sonicating MX_2 powders in ultra-pure water containing phospholipid for 12 h, followed by a centrifugation to purify the dispersions from large aggregates (full details can be found in the ESI†). We have previously described how this procedure can be applied to graphene exfoliation,[29] where we have shown that the amount of 2D-material dispersed was dependent on the phospholipid concentration and the fluidity of the phospholipid aliphatic chains. Herein, we report that the same method can be used to produce meta-stable aqueous dispersions for each TMDC tested, namely MoS_2, WS_2, TiS_2 and $MoSe_2$, as well as hBN. For the dispersions characterised in this study, MX_2 and hBN powders were sonicated in ultra-pure water with 1,2-dioleoyl-*sn*-glycero-3-phosphocholine (DOPC) at a concentration of 0.2 mg mL^{-1}, resulting in dispersed concentrations in the range of 0.01–0.1 mg mL^{-1}, depending on the 2D material used. DOPC was selected as the lipid of choice on the basis of our graphene dispersion work,[29] as the fluidity of this phospholipid chain was shown to impart a good level of dispersion stability compared to other phospholipids. Thermogravimetric analysis (TGA) performed on freeze-dried dispersions of MoS_2, WS_2 and TiS_2 suggest that the method typically produces fresh dispersions containing 10–20% weight of dispersed 2D-material (refer to Fig. S1 in the ESI†), comparable to that observed for graphene dispersions produced by the same method.[29]

Ultraviolet-visible (UV-vis) spectroscopy confirmed the presence of dispersed few-layer MX_2 species, with the following characteristic major absorption peaks: 393, 450, 608 and 665 nm for MoS_2;[3,30,31] 412, 697 and 805 nm for $MoSe_2$;[3,32] 593 nm for TiS_2[33] and 624 nm for WS_2.[3,30] No absorption peaks could be discerned from the Rayleigh scattering in the spectrum for hBN. The spectra are presented in Fig. 1A together with photographs of the dispersions.

Hydrodynamic diameter values obtained *via* dynamic light scattering (DLS) measurements are presented in Table 1, providing rough estimates (between tens and hundreds of nm, due to the approximations in the technique) of colloid size which were found to be comparable to those observed for graphene dispersions produced by the same method.[29] The dispersed TMDCs were characterized by negative ζ potential values at neutral pH (see Table 1), although smaller in magnitude to those observed for the graphene dispersions (-34 mV). Shorter-term stability is expected as a result of this observation and this is confirmed by comparison of the time-dependent reductions in optical density presented in Table 1. It is worth noting that the TiS_2 dispersions, approximately 12 h after preparation, produce a strong sulphurous odour: it is known that this material is prone to oxidation in aqueous solution, most likely *via* the following reaction:[34]
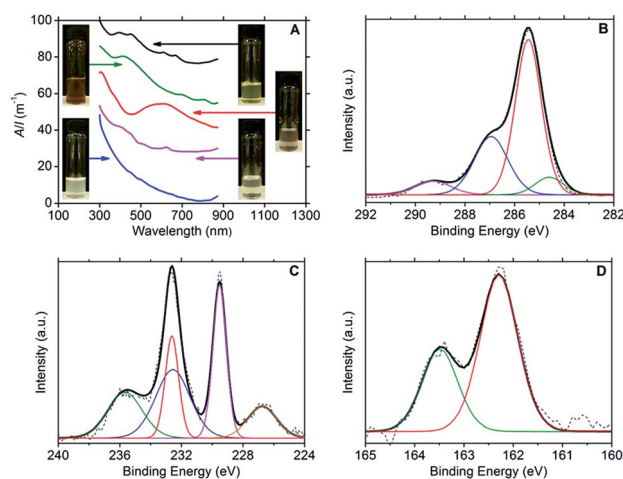

Fig. 1 (A) UV-vis absorbance spectra of the aqueous DOPC/2D-material dispersions (from top to bottom): MoS_2 (black line), $MoSe_2$ (green line), TiS_2 (red line), WS_2 (purple line) and hBN (blue line). The stacked spectra are in proportion to each other. (B) C1s XPS spectrum of a DOPC/MoS_2 dispersion drop cast onto Si/SiO$_2$ substrate. In the fitting, the green line corresponds to the C–C sp^2 peak, the red line to the C–C sp^3 peak, the blue line to the C–O/C–N peak and the purple line to the O–C=O peak. (C) Mo3d XPS spectrum of a DOPC/MoS_2 dispersion drop cast onto Si/SiO$_2$ substrate. In the fitting, the orange line corresponds to the S2s peak, the purple line to the Mo^{4+}3d$_{5/2}$ peak, the red line to the Mo^{4+}3d$_{3/2}$ peak, the blue line to the Mo^{6+}3d$_{5/2}$ peak and the green line to the Mo^{6+}3d$_{3/2}$ peak. (D) S2p XPS spectrum of a DOPC/MoS_2 dispersion drop cast onto Si/SiO$_2$ substrate. The fitting is for the S2p doublet, with the red line depicting the S2p$_{3/2}$ peak and the green line the S2p$_{1/2}$ peak.

$$TiS_2 + xH_2O \rightarrow TiS_{2-x}O_x + xH_2S$$
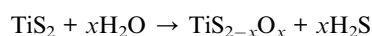
As the hBN dispersions were found to precipitate at a significantly faster rate to the other 2D materials, no further characterisation work was conducted on hBN dispersions as part of this study.

X-ray photoelectron spectroscopy (XPS) was used to confirm the presence of DOPC and MX_2 in the dispersions; refer to Fig. 1B–D (and Fig. S2–S4 in the ESI†). For DOPC, the C1s spectrum for all samples (dispersions of MoS_2, $MoSe_2$, WS_2 and TiS_2) showed peaks representatives of DOPC at average binding energies of 284.5 eV (C–C sp^2), 285.3 eV (C–C sp^3), 286.9 eV (combined signal for C–O and C–N) and 289.2 eV (O–C=O).[29] Furthermore, the phosphorous and nitrogen peaks were found to be present at similar percentage atomic concentrations appearing at average binding energies of 134.0 eV and 134.9 eV (P2p$_{3/2}$ and P2p$_{1/2}$) and 402.9 eV respectively (N1s). For MoS_2, the Mo3d$_{3/2}$ and Mo3d$_{5/2}$ doublet peaks were located at 232.6 eV and 229.5 eV respectively, with the S2s peak at 226.7 eV and the S2p doublet at 163.5 eV and 162.3 eV (S2p$_{1/2}$ and S2p$_{3/2}$). These binding energies are indicative of the expected Mo^{4+} and S^{2-} chemical states.[35–38] However, the presence of a peak at 235.6 eV is indicative of the Mo3d$_{3/2}$ doublet peak for Mo^{6+}, and fitting reveals the complementary Mo3d$_{5/2}$ peak at 232.5 eV, which strongly suggests that MoO_3 is present at approximately the same concentration as MoS_2 (percentage atomic concentrations

Table 1 Summary of ζ potential and DLS hydrodynamic diameter values (*D*) as measured for various 2D-material/DOPC aqueous dispersions, as well as stability data in the form of reduction in optical density *versus* day 0 (ODR)

Material	ζ (mV)	*D* (nm)	ODR day 10[a]	ODR day 20[a]	ODR day 30[a]	ODR day 50[a]
MoS_2	−20	142	8%	16%	32%	71%
$MoSe_2$	−28	164	14%	23%	34%	87%
TiS_2	−19	495	56%	69%	81%	92%
WS_2	−15	255	14%	29%	51%	85%
hBN	−23	295	70%	74%	80%	85%
Graphene	−34	190	—	11%[b]	25%[b]	43%[b]

[a] Optical density measured at A_{608} (MoS_2), A_{805} ($MoSe_2$), A_{565} (TiS_2), A_{624} (WS_2), A_{300} (hBN) and A_{660} (graphene), where subscripts are wavelengths in nanometres. Graphene data at A_{660} taken from ref. 29. [b] Optical density data for graphene measured at A_{660} at time points: 22, 41 and 56 days.

of 47% Mo^{4+} and 53% Mo^{6+}).[37–40] The Mo^{6+} state was more heavily detected for the $MoSe_2$ dispersions (percentage atomic concentrations of 11% Mo^{4+} and 89% Mo^{6+}). The $Mo3d_{3/2}$ and $Mo3d_{5/2}$ doublet peaks for Mo^{6+} appear at 236.1 eV and 232.9 eV respectively, the same doublet peaks for Mo^{4+} being found at lower intensities at 232.5 eV and 229.4 eV, with the $Se3d_{3/2}$ and $Se3d_{5/2}$ doublet peaks appearing at 56.6 eV and 55.8 eV.[36] For WS_2, two chemical states were also detected for tungsten, W^{4+} and W^{6+}. The $W4f_{5/2}$ and $W4f_{7/2}$ doublet peaks expected for WS_2 are observed at 34.6 eV and 32.7 eV with the $S2p$ doublet peaks appearing at 163.4 eV and 162.2 eV ($S2p_{1/2}$ and $S2p_{3/2}$). The $W4f_{5/2}$ and $W4f_{7/2}$ doublet peaks characteristic of the W^{6+} chemical state are seen at 38.1 eV and 36.0 eV, and represent the dominant binding energies of the $W4f$ signal (percentage atomic concentrations of 12% W^{4+} and 88% W^{6+}),[35,36,41] which coupled with the weak $S2p$ signal suggests that the samples contained significant amounts of WO_3. For TiS_2, the $Ti2p_{1/2}$ and $Ti2p_{3/2}$ doublet peaks appear at 464.8 eV and 459.1 eV respectively, with the $S2p$ doublet peaks appearing at 165.2 eV and 163.9 eV ($S2p_{1/2}$ and $S2p_{3/2}$). These binding energies are indicative of the expected Ti^{4+} and $S^{2−}$ chemical states.[42,43] However, as with that observed for the WS_2 sample, a weak $S2p$ signal intensity was observed when compared to the $Ti2p$ signal intensity. This observation, in conjunction with the dispersion stability data, suggests that oxidised titanium is also present in significant quantity. The partial oxidation of the TMDCs, detected by the XPS, could explain the lower long-term stability of the DOPC-stabilised dispersions relative to the graphene sample (see Table 1). Consistent with this, it is noted that the TiS_2 sample has the lowest level of dispersion stability.

Raman spectroscopy was used to further characterise the DOPC/MX_2 dispersions and to confirm the presence of few-layer flakes. Analysis was performed on drop-cast samples using Si/SiO₂ substrates. For MoS_2, spectra diagnostic of few-layer flakes predominated with the A_{1g} and E^1_{2g} typically appearing at 406 cm⁻¹ and 382 cm⁻¹ respectively, separated by 24 cm⁻¹, yielding maximum photoluminescent (PL) emission at 675 nm (1.84 eV), which is consistent with literature values for few-layer MoS_2.[44–49] Similarly, the spectra measured for the WS_2 samples were found to be representative of few-layer material,[47–52] with A_{1g} and E^1_{2g} appearing at 419 cm⁻¹ and 351 cm⁻¹ respectively, separated by 68 cm⁻¹ and yielding maximum photoluminescent (PL) emission at 633 nm (1.96 eV). Few-layer flakes

were also detected for $MoSe_2$ and TiS_2. For $MoSe_2$, this was confirmed by the following representative peaks: 351 cm⁻¹ (B^1_{2g}), 285 cm⁻¹ (E^2_{2g}) and 241 cm⁻¹ (A_{1g})[48,49,53] and for TiS_2: 377 cm⁻¹ (A_{2u}), 333 cm⁻¹ (A_{1g}) and 233 cm⁻¹ (E_g),[33,49,54] with the $A_{1g} : A_{2u}$ peak intensity ratio at approximately 2.0 (compare to a value of 1.6 measured for the bulk powder starting-material).[33] Weaker PL emissions were observed for the samples derived from the $MoSe_2$ and TiS_2 dispersions, as compared to those
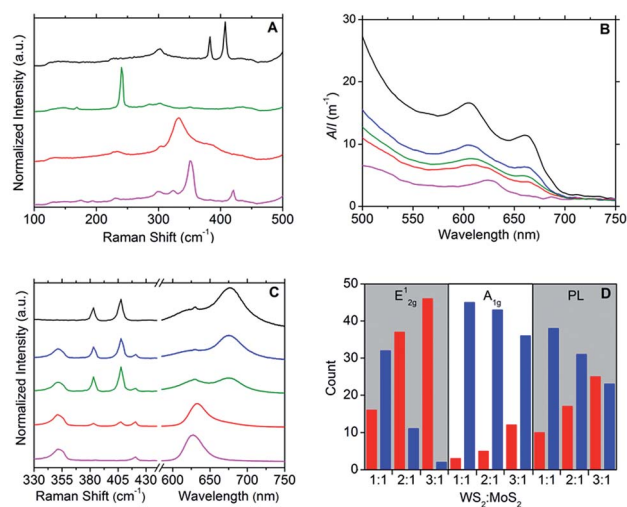

Fig. 2 (A) Raman spectra (532 nm excitation) of the DOPC/MX_2 dispersions drop cast onto Si/SiO₂ substrates, corresponding (from top to bottom) to MoS_2 (black line), $MoSe_2$ (green line), TiS_2 (red line) and WS_2 (purple line). (B) UV-vis spectra of the following aqueous DOPC/2D-material dispersions (from top to bottom): MoS_2 (black line), 1 : 1 WS_2 : MoS_2 heterostructures (blue line), 2 : 1 WS_2 : MoS_2 heterostructures (green line), 3 : 1 WS_2 : MoS_2 heterostructures (red line) and WS_2 (purple line). (C) Typical Raman and PL spectra (532 nm excitation) measured for the following DOPC/2D-material dispersions drop cast onto Si/SiO₂ substrates (from top to bottom): MoS_2 (black line), 1 : 1 WS_2 : MoS_2 heterostructures (blue line), 2 : 1 WS_2 : MoS_2 heterostructures (green line), 3 : 1 WS_2 : MoS_2 heterostructures (red line) and WS_2 (purple line). (D) Histograms showing the relative proportions of dominant peak intensities in the Raman (E^1_{2g} and A_{1g}) and PL spectra (λ_{max}) of aqueous DOPC-mediated dispersions of 1 : 1, 2 : 1 and 3 : 1 WS_2 : MoS_2 heterostructures. Instances where the peak intensities arising from WS_2 are greater than those from MoS_2 are binned on the left-hand side (red columns) with the converse case binned on the right-hand side (blue columns); a bin size of 48 measurements (at different sample spots) was used in all instances.

from MoS$_2$ and WS$_2$ dispersions. Fig. 2A and S5–S8 in the ESI† give typical examples of the Raman and PL spectra measured.

Finally, atomic force microscopy (AFM) performed on drop-cast samples of DOPC/MoS$_2$ dispersions (clean mica substrates were used) showed structures similar to those observed for graphene dispersions produced by the same method,[29] with an average height of 40 nm. The AFM height images showed objects characterized by "steps" with a height of 5 nm (or multiple of 5 nm), which is a thickness comparable to that of a DOPC bilayer;[55–58] refer to Fig. S9 in the ESI† for further details.

Supplemental to the novel properties offered by true 2D materials and their few-layer counterparts, mixed van der Waals stacking of different 2D materials to form heterostructures, endow few-layer materials with scope to impart bespoke properties.[2,9–11,38,59] In addition to our method detailed above for the production of aqueous DOPC/MX$_2$ dispersions, we also present a fast and single-step method to prepare aqueous DOPC/heterostructure dispersions. Briefly, the method involves mixing the desired parent DOPC/MX$_2$ dispersions at specific volume ratios, after which the mixtures are sonicated for 10 minutes to facilitate the de-stacking and subsequent re-stacking of the parent layers into hetero-layered stacks. The method was used to prepare aqueous DOPC/WS$_2$: MoS$_2$ dispersions, where the resulting optoelectronic properties were found to be tuneable to the relative quantities of the parent dispersions used. UV-vis spectroscopy (Fig. 2B) was used as a simple screening tool for the selection of appropriate volume ratios of DOPC/WS$_2$ (x) and DOPC/MoS$_2$ (y) dispersions to produce heterostructure dispersions with desired optoelectronic properties. For example, the UV-vis spectrum of the DOPC/WS$_2$: MoS$_2$ dispersion prepared using the $x : y$ ratio at 2 : 1 was found to be intermediate in character between those of the parent dispersions, with flakes (deposited on Si/SiO$_2$ substrates) also displaying intermediate character with regard to Raman and PL response; refer to Fig. 2C. Further illustration of this optoelectronic tuning is shown via the histograms presented in Fig. 2D, which are based on Raman and PL data measured from a total of 48 flakes per DOPC/WS$_2$: MoS$_2$ dispersion ($x : y$ ratio at 1 : 1, 2 : 1 and 3 : 1). The measured flakes were categorised into two conditions: one where the Raman (A$_{1g}$ and E$_{2g}^1$) and PL (λ_{max}) intensities were greater for peaks emanating from WS$_2$ (approximately 419 cm^{-1} for A$_{1g}$, 350 cm^{-1} for E$_{2g}^1$ and 633 nm for PL) and the other where the intensities were greater for peaks emanating from MoS$_2$ (approximately 407 cm^{-1} for A$_{1g}$, 383 cm^{-1} for E$_{2g}^1$ and 675 nm for PL). As expected, the intensities of the peaks arising from WS$_2$ become greater as x increases and as such, the findings show that manipulation of the $x : y$ volume ratio allows for the tuning of the predominant optoelectronic properties of heterostructure flakes.

Conclusions

In summary, a simple method has been presented to produce aqueous dispersions of phospholipid-coated few-layer transition-metal dichalcogenides (MoS$_2$, WS$_2$, TiS$_2$ and MoSe$_2$) via single-step exfoliation of the bulk starting materials in

water. Furthermore, the resulting dispersions can be subsequently mixed at pre-defined volume ratios to produce heterostructured dispersions thereby allowing for the tuning of the optoelectronic properties. The phospholipid coating renders the flakes biofunctional, which coupled with the unique properties of transition-metal dichalcogenides, indicates the great potential of this method for use in biological applications, for example in vivo sensing or drug transport.

Conflicts of interest

The authors declare no conflict of interest.

Acknowledgements

Notes and references

1 S. Z. Butler, S. M. Hollen, L. Y. Cao, Y. Cui, J. A. Gupta, H. R. Gutierrez, T. F. Heinz, S. S. Hong, J. X. Huang, A. F. Ismach, E. Johnston-Halperin, M. Kuno, V. V. Plashnitsa, R. D. Robinson, R. S. Ruoff, S. Salahuddin, J. Shan, L. Shi, M. G. Spencer, M. Terrones, W. Windl and J. E. Goldberger, ACS Nano, 2013, 7, 2898–2926.

2 X. P. Hong, J. Kim, S. F. Shi, Y. Zhang, C. H. Jin, Y. H. Sun, S. Tongay, J. Q. Wu, Y. F. Zhang and F. Wang, Nat. Nanotechnol., 2014, 9, 682–686.

3 Q. H. Wang, K. Kalantar-Zadeh, A. Kis, J. N. Coleman and M. S. Strano, Nat. Nanotechnol., 2012, 7, 699–712.

4 M. L. Tsai, S. H. Su, J. K. Chang, D. S. Tsai, C. H. Chen, C. I. Wu, L. J. Li, L. J. Chen and J. H. He, ACS Nano, 2014, 8, 8317–8322.

5 E. G. D. Firmiano, A. C. Rabelo, C. J. Dalmaschio, A. N. Pinheiro, E. C. Pereira, W. H. Schreiner and E. R. Leite, Adv. Energy Mater., 2014, 4, 1301380.

6 G. H. Lee, Y. J. Yu, X. Cui, N. Petrone, C. H. Lee, M. S. Choi, D. Y. Lee, C. Lee, W. J. Yoo, K. Watanabe, T. Taniguchi, C. Nuckolls, P. Kim and J. Hone, ACS Nano, 2013, 7, 7931–7936.

7 M. Chhowalla, H. S. Shin, G. Eda, L. J. Li, K. P. Loh and H. Zhang, Nat. Chem., 2013, 5, 263–275.

8 R. Mas-Balleste, C. Gomez-Navarro, J. Gomez-Herrero and F. Zamora, Nanoscale, 2011, 3, 20–30.

9 C. M. Huang, S. F. Wu, A. M. Sanchez, J. J. P. Peters, R. Beanland, J. S. Ross, P. Rivera, W. Yao, D. H. Cobden and X. D. Xu, Nat. Mater., 2014, 13, 1096–1101.

10 H. Fang, C. Battaglia, C. Carraro, S. Nemsak, B. Ozdol, J. S. Kang, H. A. Bechtel, S. B. Desai, F. Kronast, A. A. Unal, G. Conti, C. Conlon, G. K. Palsson, M. C. Martin, A. M. Minor, C. S. Fadley, E. Yablonovitch, R. Maboudian

and A. Javey, *Proc. Natl. Acad. Sci. U. S. A.*, 2014, **111**, 6198–6202.

11 H. Wang, F. C. Liu, W. Fu, Z. Y. Fang, W. Zhou and Z. Liu, *Nanoscale*, 2014, **6**, 12250–12272.

12 D. J. Finn, M. Lotya, G. Cunningham, R. J. Smith, D. McCloskey, J. F. Donegan and J. N. Coleman, *J. Mater. Chem. C*, 2014, **2**, 925–932.

13 Y. Hernandez, V. Nicolosi, M. Lotya, F. M. Blighe, Z. Y. Sun, S. De, I. T. McGovern, B. Holland, M. Byrne, Y. K. Gun'ko, J. J. Boland, P. Niraj, G. Duesberg, S. Krishnamurthy, R. Goodhue, J. Hutchison, V. Scardaci, A. C. Ferrari and J. N. Coleman, *Nat. Nanotechnol.*, 2008, **3**, 563–568.

14 U. Khan, A. O'Neill, M. Lotya, S. De and J. N. Coleman, *Small*, 2010, **6**, 864–871.

15 J. N. Coleman, M. Lotya, A. O'Neill, S. D. Bergin, P. J. King, U. Khan, K. Young, A. Gaucher, S. De, R. J. Smith, I. V. Shvets, S. K. Arora, G. Stanton, H. Y. Kim, K. Lee, G. T. Kim, G. S. Duesberg, T. Hallam, J. J. Boland, J. J. Wang, J. F. Donegan, J. C. Grunlan, G. Moriarty, A. Shmeliov, R. J. Nicholls, J. M. Perkins, E. M. Grieveson, K. Theuwissen, D. W. McComb, P. D. Nellist and V. Nicolosi, *Science*, 2011, **331**, 568–571.

16 A. O'Neill, U. Khan and J. N. Coleman, *Chem. Mater.*, 2012, **24**, 2414–2421.

17 T. C. Hernandez, A. C. F. Blanco, A. T. Williams, M. Velicky, H. V. Patten, A. Colina and R. A. W. Dryfe, *Electroanalysis*, 2015, **27**, 1026–1034.

18 J. Zheng, H. Zhang, S. H. Dong, Y. P. Liu, C. T. Nai, H. S. Shin, H. Y. Jeong, B. Liu and K. P. Loh, *Nat. Commun.*, 2014, **5**, 2995.

19 X. Huang, Z. Y. Zeng and H. Zhang, *Chem. Soc. Rev.*, 2013, **42**, 1934–1946.

20 R. A. Gordon, D. Yang, E. D. Crozier, D. T. Jiang and R. F. Frindt, *Phys. Rev. B*, 2002, **65**, 125407.

21 L. Zhou, B. Z. He, Y. Yang and Y. G. He, *RSC Adv.*, 2014, **4**, 32570–32578.

22 G. Cunningham, M. Lotya, C. S. Cucinotta, S. Sanvito, S. D. Bergin, R. Menzel, M. S. P. Shaffer and J. N. Coleman, *ACS Nano*, 2012, **6**, 3468–3480.

23 N. B. Vargaftik, B. N. Volkov and L. D. Voljak, *J. Phys. Chem. Ref. Data*, 1983, **12**, 817–820.

24 R. J. Smith, P. J. King, M. Lotya, C. Wirtz, U. Khan, S. De, A. O'Neill, G. S. Duesberg, J. C. Grunlan, G. Moriarty, J. Chen, J. Z. Wang, A. I. Minett, V. Nicolosi and J. N. Coleman, *Adv. Mater.*, 2011, **23**, 3944–3948.

25 Y. G. Yao, L. Tolentino, Z. Z. Yang, X. J. Song, W. Zhang, Y. S. Chen and C. P. Wong, *Adv. Funct. Mater.*, 2013, **23**, 3577–3583.

26 M. D. J. Quinn, N. H. Ho and S. M. Notley, *ACS Appl. Mater. Interfaces*, 2013, **5**, 12751–12756.

27 L. Guardia, J. I. Paredes, R. Rozada, S. Villar-Rodil, A. Martinez-Alonso and J. M. D. Tascon, *RSC Adv.*, 2014, **4**, 14115–14127.

28 A. Gupta, V. Arunachalam and S. Vasudevan, *J. Phys. Chem. Lett.*, 2015, **6**, 739–744.

29 A. T. Williams, R. Donno, N. Tirelli and R. A. W. Dryfe, *RSC Adv.*, 2018, **8**, 19220–19225.

30 T. P. Nguyen, W. Sohn, J. H. Oh, H. W. Jang and S. Y. Kim, *J. Phys. Chem. C*, 2016, **120**, 10078–10085.

31 I. Bilgin, F. Liu, A. Vargas, A. Winchester, M. K. L. Man, M. Upmanyu, K. M. Dani, G. Gupta, S. Talapatra, A. D. Mohite and S. Kar, *ACS Nano*, 2015, **9**, 8822–8832.

32 N. Berahim, I. S. Amiri, T. Anwar, S. R. Azzuhri, M. N. S. Mohd Nasir, R. Zakaria, W. Y. Chong, C. K. Lai, S. H. Lee, H. Ahmad, M. A. Ismail and P. Yupapin, *Results Phys.*, 2019, **12**, 7–11.

33 P. C. Sherrell, K. Sharda, C. Grotta, J. Ranalli, M. S. Sokolikova, F. M. Pesci, P. Palczynski, V. L. Bemmer and C. Mattevi, *ACS Omega*, 2018, **3**, 8655–8662.

34 E. Long, S. O'Brien, E. A. Lewis, E. Prestat, C. Downing, C. S. Cucinotta, S. Sanvito, S. J. Haigh and V. Nicolosi, *npj 2D Mater. Appl.*, 2017, **1**, 22.

35 M.-H. Chiu, C. Zhang, H.-W. Shiu, C.-P. Chuu, C.-H. Chen, C.-Y. S. Chang, C.-H. Chen, M.-Y. Chou, C.-K. Shih and L.-J. Li, *Nat. Commun.*, 2015, **6**, 7666.

36 J. Guo, Y. Shi, X. Bai, X. Wang and T. Ma, *J. Mater. Chem. A*, 2015, **3**, 24397–24404.

37 G. Tai, T. Zeng, J. Yu, J. Zhou, Y. You, X. Wang, H. Wu, X. Sun, T. Hu and W. Guo, *Nanoscale*, 2016, **8**, 2234–2241.

38 Z. Lin, B. R. Carvalho, E. Kahn, R. Lv, R. Rao, H. Terrones, M. A. Pimenta and M. Terrones, *2D Materials*, 2016, **3**, 022002.

39 H. Nan, Z. Wang, W. Wang, Z. Liang, Y. Lu, Q. Chen, D. He, P. Tan, F. Miao, X. Wang, J. Wang and Z. Ni, *ACS Nano*, 2014, **8**, 5738–5745.

40 V. Madhavi, P. Kondaiah, S. S. Rayudu, O. M. Hussain and S. Uthanna, *Mater. Express*, 2013, **3**, 135–143.

41 K. M. McCreary, A. T. Hanbicki, G. G. Jernigan, J. C. Culbertson and B. T. Jonker, *Sci. Rep.*, 2016, **6**, 19159.

42 C. Lin, X. Zhu, J. Feng, C. Wu, S. Hu, J. Peng, Y. Guo, L. Peng, J. Zhao, J. Huang, J. Yang and Y. Xie, *J. Am. Chem. Soc.*, 2013, **135**, 5144–5151.

43 D. Tonti, C. Pettenkofer and W. Jaegermann, *Electrochem. Solid-State Lett.*, 2000, **3**(5), 220–223.

44 R. Ganatra and Q. Zhang, *ACS Nano*, 2014, **8**, 4074–4099.

45 K. F. Mak, C. Lee, J. Hone, J. Shan and T. F. Heinz, *Phys. Rev. Lett.*, 2010, **105**, 136805.

46 A. Splendiani, L. Sun, Y. Zhang, T. Li, J. Kim, C.-Y. Chim, G. Galli and F. Wang, *Nano Lett.*, 2010, **10**, 1271–1275.

47 M. A. Bissett, A. G. Hattle, A. J. Marsden, I. A. Kinloch and R. A. W. Dryfe, *ACS Omega*, 2017, **2**, 738–745.

48 Y. Niu, S. Gonzalez-Abad, R. Frisenda, P. Marauhn, M. Drüppel, P. Gant, R. Schmidt, S. N. Taghavi, D. Barcons, J. A. Molina-Mendoza, M. S. De Vasconcellos, R. Bratschitsch, D. Perez De Lara, M. Rohlfing and A. Castellanos-Gomez, *Nanomaterials*, 2018, **8**, 725.

49 M. Bissett, S. Worrall, I. Kinloch and R. A. W. Dryfe, *Electrochim. Acta*, 2016, **201**, 30–37.

50 W. Zhao, Z. Ghorannevis, L. Chu, M. Toh, C. Kloc, P.-H. Tan and G. Eda, *ACS Nano*, 2013, **7**, 791–797.

51 A. Berkdemir, H. R. Gutiérrez, A. R. Botello-Méndez, N. Perea-López, A. L. Elías, C.-I. Chia, B. Wang, V. H. Crespi, F. López-Urías, J.-C. Charlier, H. Terrones and M. Terrones, *Sci. Rep.*, 2013, **3**, 1755.

52 G. V. Bianco, M. Losurdo, M. M. Giangregorio, A. Sacchetti, P. Prete, N. Lovergine, P. Capezzuto and G. Bruno, *RSC Adv.*, 2015, **5**, 98700–98708.

53 P. Tonndorf, R. Schmidt, P. Böttger, X. Zhang, J. Börner, A. Liebig, M. Albrecht, C. Kloc, O. Gordan, D. R. T. Zahn, S. Michaelis de Vasconcellos and R. Bratschitsch, *Opt. Express*, 2013, **21**, 4908–4916.

54 K. Dolui and S. Sanvito, *Europhys. Lett.*, 2016, **115**, 47001.

55 M. Hirtz, A. Oikonomou, T. Georgiou, H. Fuchs and A. Vijayaraghavan, *Nat. Commun.*, 2013, **4**, 2591.

56 S. T. Wang, M. Fukuto and L. Yang, *Phys. Rev. E: Stat., Nonlinear, Soft Matter Phys.*, 2008, **77**, 031909.

57 A. Dols-Perez, L. Fumagalli and G. Gomila, *Colloids Surf., B*, 2014, **116**, 295–302.

58 Z. V. Leonenko, E. Finot, H. Ma, T. E. S. Dahms and D. T. Cramb, *Biophys. J.*, 2004, **86**, 3783–3793.

59 L. Liang and V. Meunier, *Nanoscale*, 2014, **6**, 5394–5401.